Generation and evaluation of protease inhibitor-resistant SARS-CoV-2 strains

Hawa Sophia Bouzidi[1,#], Jean-Sélim Driouich[1,#], Raphaëlle Klitting[1,#], Ornéllie Bernadin[1], Géraldine Piorkowski[1], Rayane Amaral[1], Laurent Fraisse[2], Charles E. Mowbray[2], Ivan Scandale[2], Fanny Escudié[2], Eric Chatelain[2], Xavier de Lamballerie[1,], Antoine Nougairède[1], and Franck Touret[1,*].

[1]: Unité des Virus Émergents, UVE : Aix Marseille Univ, IRD 190, INSERM 1207, Marseille, France

[2] : Drugs for Neglected Diseases initiative, Geneva, Switzerland

# These authors contributed equally to this work

*Corresponding author: franck.touret@univ-amu.fr

Highlights

- SARS-CoV-2 resistant strains to clinical stage protease inhibitors have been generated after 16 passages *in vitro*
- The ensitrelvir resistance mutation M49L induces a strong resistance to ensitrelvir *in vitro* in three different isolates
- M49L mutation alone renders ensitrelvir treatment ineffective *in vivo*
- The prevalence of naturally occurring M49L-mutants has increased over recent months

Abstract

Since the start of the SARS-CoV-2 pandemic, the search for antiviral therapies has been at the forefront of medical research. To date, the 3CLpro inhibitor nirmatrelvir (Paxlovid®) has shown the best results in clinical trials and the greatest robustness against variants. A second SARS-CoV-2 protease inhibitor, ensitrelvir (Xocova®), has been developed. Ensitrelvir, currently in Phase 3, was approved in Japan under the emergency regulatory approval procedure in November 2022, and is available since March 31, 2023. One of the limitations for the use of antiviral monotherapies is the emergence of resistance mutations. Here, we experimentally generated mutants resistant to nirmatrelvir and ensitrelvir *in vitro* following repeating passages of SARS-CoV-2 in the presence of both antivirals. For both molecules, we demonstrated a loss of sensitivity for resistance mutants *in vitro*. Using a Syrian golden hamster infection model, we showed that the ensitrelvir M49L mutation confers a high level of *in vivo* resistance. Finally, we identified a recent increase in the prevalence of M49L-carrying sequences, which appears to be associated with multiple repeated emergence events in Japan and may be related to the use of Xocova® in the country since November 2022. These results highlight the strategic importance of genetic monitoring of circulating SARS-CoV-2 strains to ensure that treatments administered retain their full effectiveness.

Keywords

COVID-19, SARS-CoV-2, antiviral therapy, protease inhibitors, resistance

Introduction

Since the beginning of the SARS-CoV-2 pandemic in 2020, the search for antiviral therapeutics has been a major focus for medical research. As previously observed with Influenza and HIV, effective countermeasures to treat people can be decisive in managing a health crisis. At the start of the pandemic, the repositioning of broad-spectrum antivirals targeting the replication complex raised great expectations(Wang *et al*, 2020; Williamson *et al*, 2020), which were dashed by disappointing results in clinical trials(Beigel *et al*, 2020). Therapeutic antibodies have subsequently demonstrated their usefulness(Starr *et al*, 2021; Pinto *et al*, 2020), but failed to overcome the emergence of variants escaping the humoral response(Touret *et al*, 2023). Ultimately, the best effects in clinical trials(Hammond *et al*, 2022) and the greatest robustness against variants(Vangeel *et al*, 2022) were achieved with the protease inhibitor nirmatrelvir(Owen *et al*, 2021) (PF-07321332, Paxlovid®), targeting the 3CLpro. This inhibitor of the coronavirus protease 3CLpro (PF-00835231) was originally developed against SARS-CoV-1. It is also effective against SARS-CoV-2 by preventing the cleavage of the polyproteins PP1a and PP1ab – effectively blocking the generation of the non-structural proteins essential for viral replication(Jin *et al*, 2020).
The pharmacokinetics (PK) of nirmatrelvir, whose metabolism includes a predominant role for CYP3A4(Owen *et al*, 2021), have been improved by the combination with ritonavir used as a exposure booster. However, this combination may complicate the use of nimatrelvir in certain patients receiving other drugs whose metabolism may also be modified by ritonavir(Hoertel *et al*, 2022).

In the meantime, a second SARS-CoV-2 3CLpro inhibitor named ensitrelvir (S-217622), was developed by the Japanese company Shionogi. The molecule was identified through a combination of virtual and biological screenings followed by optimization using a structure-based drug design strategy(Unoh *et al*, 2022). It has been proposed for use without an association with ritonavir(Unoh *et al*, 2022). Following encouraging results in Phase 2 clinical trials, it is now in Phase 3(University of Minnesota, 2023; Shionogi, 2023). In Japan, however, ensitrelvir (Xocova®), was approved under the emergency regulatory approval procedure in November 2022 and has been available on prescription since March 31, 2023.

Resistance mutations can represent a major limitation to the use of antiviral mono-therapies. Such mutations may naturally be observed in a proportion of circulating strains in the absence of any apparent specific selective pressure(Kawashima *et al*, 2023; Ip *et al*, 2023; Bloom *et al*, 2010) and/or appear in patients in the context of conditions of use associated with sub-optimal efficiency (e.g., during prolonged use in a patient with long lasting viral replication). For instance, the emergence of resistance against antiviral monotherapy has been observed in patients treated with the monoclonal antibody sotrovimab during the Delta wave of SARS-CoV-2(Rockett *et al*, 2022).

Here, we experimentally generated nirmatrelvir and ensitrelvir resistance mutants. For both molecules, we demonstrated a loss in sensitivity for the resistance mutants *in vitro.* Using a Syrian golden hamster model of SARS-CoV-2 infection, we showed that the ensitrelvir resistance mutation M49L confers a high level of resistance *in vivo*. Finally, we identified a

recent increase in the prevalence of M49L-carrying sequences, that we link to multiple repeated emergence events in Japan, and may be associated with the commercialization of the molecule in the country since April 2023.

Results

Generation of SARS-CoV-2 strains resistant to protease inhibitors

To generate mutants resistant to SARS-CoV-2 protease inhibitors, we first determined the experimental conditions suitable for the emergence of such resistance mutations in cell culture. We evaluated, for both molecules, the half maximal effective concentration EC_{50} in the VeroE6 TMPRSS2 cell line, using remdesivir as a reference compound and the BavPat1 SARS-CoV-2 strain (B.1 lineage carrying the D614G mutation). In line with the literature(Imai *et al*, 2022; Takashita *et al*, 2022; Sasaki *et al*, 2022; Unoh *et al*, 2022), we obtained EC_{50s} of 0.14µM and 2.26µM for ensitrelvir and nirmatrelvir, respectively (Fig1a).

Erreur ! Signet non défini. Then, for each of the compounds, we started to grow the virus at the EC_{50}, doubling the drug amount every two passages to increase selective pressure while allowing the virus to replicate (Fig1b). In parallel, we performed virus passages in the absence of antiviral molecules to identify cell line adaptation mutations. We performed the experiment with 3 replicates of each condition. To assess the emergence of potential resistance mutations at passage 8, we sequenced the NSP5 gene -which contains the 3CLpro region- but found no mutations. As it was not possible to further increase the concentration of antiviral molecule in the supernatant, we carried out 8 additional passages at the maximum concentration (8 times higher than the EC_{50}). Throughout the experiment, we were able to maintain a stable level of viral replication without any remarkable drop in viral load (Fig. 1c).

By sequencing full viral genomes from all experimental conditions at passage 16, we identified mutations in the 3CLpro region, including some that were conserved across all replicates (Fig1d).

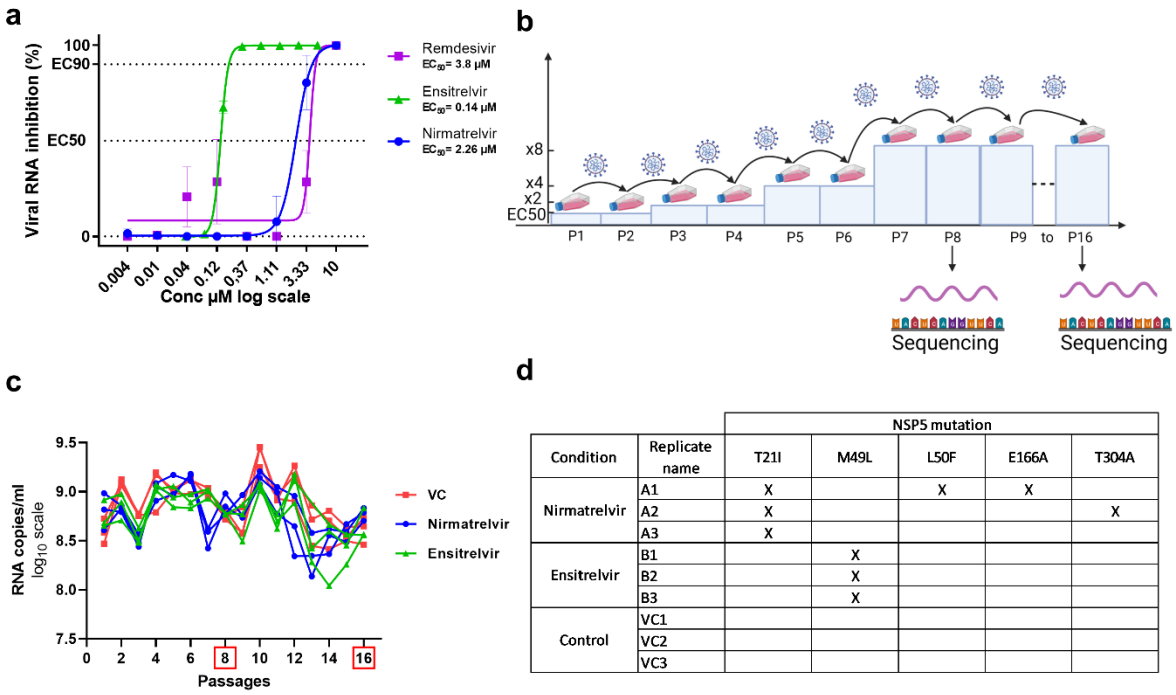

Condition	Replicate name	NSP5 mutation				
		T21I	M49L	L50F	E166A	T304A
Nirmatrelvir	A1	X		X	X	
	A2	X				X
	A3	X				
Ensitrelvir	B1		X			
	B2		X			
	B3		X			
Control	VC1					
	VC2					
	VC3					

Figure 1: Generation of nirmatrelvir and ensitrelvir resistant strains.
a) Pilot experiment to determine the EC_{50s} of nirmatrelvir and ensitrelvir. b) Graphical representation of the strategy used to obtain resistant strains. c) Viral replication measured by the amount of viral RNA at each passage in each replicate. d) Table of NSP5 amino acid mutations obtained at passage 16 in the different replicates

All three replicates of the cultures performed in the presence of nirmatrelvir exhibited the T21I mutation. The other mutations -T304A, L50F, E166A- were observed in one out of three replicates. We observed T21I either alone (replicate A3), combined with T304A (A2), or combined with both L50F and E166A (A1). All four mutations have been previously described as conferring nimatrelvir resistance(Kawashima *et al*, 2023; Iketani *et al*, 2023).
In the case of ensitrelvir, we only observed a single mutation, M49L, conserved across the three replicates. This mutation has already been described both in clinical isolates(Kawashima *et al*, 2023; Ip *et al*, 2023) and following experiments conducted *in vitro* (Kiso *et al*, 2023b) and shown to reduce sensitivity to the drug.

In vitro characterization of resistant strains

To characterize our mutant strains *in vitro*, we first monitored viral replication in VeroE6 TMPRSS2 cells in the absence of compound (Fig.2a), using a low MOI (0.02), and a RT-qPCR assay. Based on molecular viral load, we found no significant difference among the strains tested. These results are in line with the literature(Iketani *et al*, 2023) and indicate that the mutations emerged in cell culture in the presence of nirmatrelvir and ensitrelvir do not alter significantly *in vitro* replication (Fig.2a)
Using a dose-response approach, we then characterized the sensitivity of these strains to the two protease inhibitors, using remdesivir as a control. In addition to our wild-type reference strain (BavPat), we tested one of the strains that had undergone the same number of passages as the resistance mutants but without inhibitors (VC3). For the remdesivir control, we

obtained very similar EC_{50} values for the 8 viruses tested, with a maximum variation of 0.5µM in their EC_{50} (Fig 2d, Table 1). This indicates that the 16 passages in culture did not alter the sensitivity of the strains to remdesivir or their basic replication properties.

In the ensitrelvir sensitivity analysis, the VC3 strain at 16 passages showed a sensitivity very close to that of the BavPat strain, with an EC_{50} of 0.49µM versus 0.51µM. This rules out an effect of the number of passages on sensitivity (Fig. 2b, Table 1). Strains selected in the presence of nirmatrelvir (nirmatrelvirR) showed a slightly reduced sensitivity to ensitrelvir (3 to 9-fold). On the other hand, the three M49L ensitrelvir-resistant (ensitrelvirR) mutants showed a great decrease in sensitivity (around 40-fold), indicating that this mutation does confer resistance to ensitrelvir (Fig. 2b, Table 1).

In the nirmatrelvir sensitivity analysis, the VC3 strain showed a sensitivity close to that of the BavPat strain, with an EC_{50} of 4.82µM versus 3.70µM (Fig. 2cTable 1). As before, two profiles were observed for the mutant strains (Fig. 2cTable 1): ensitrelvirR strains showed a slightly

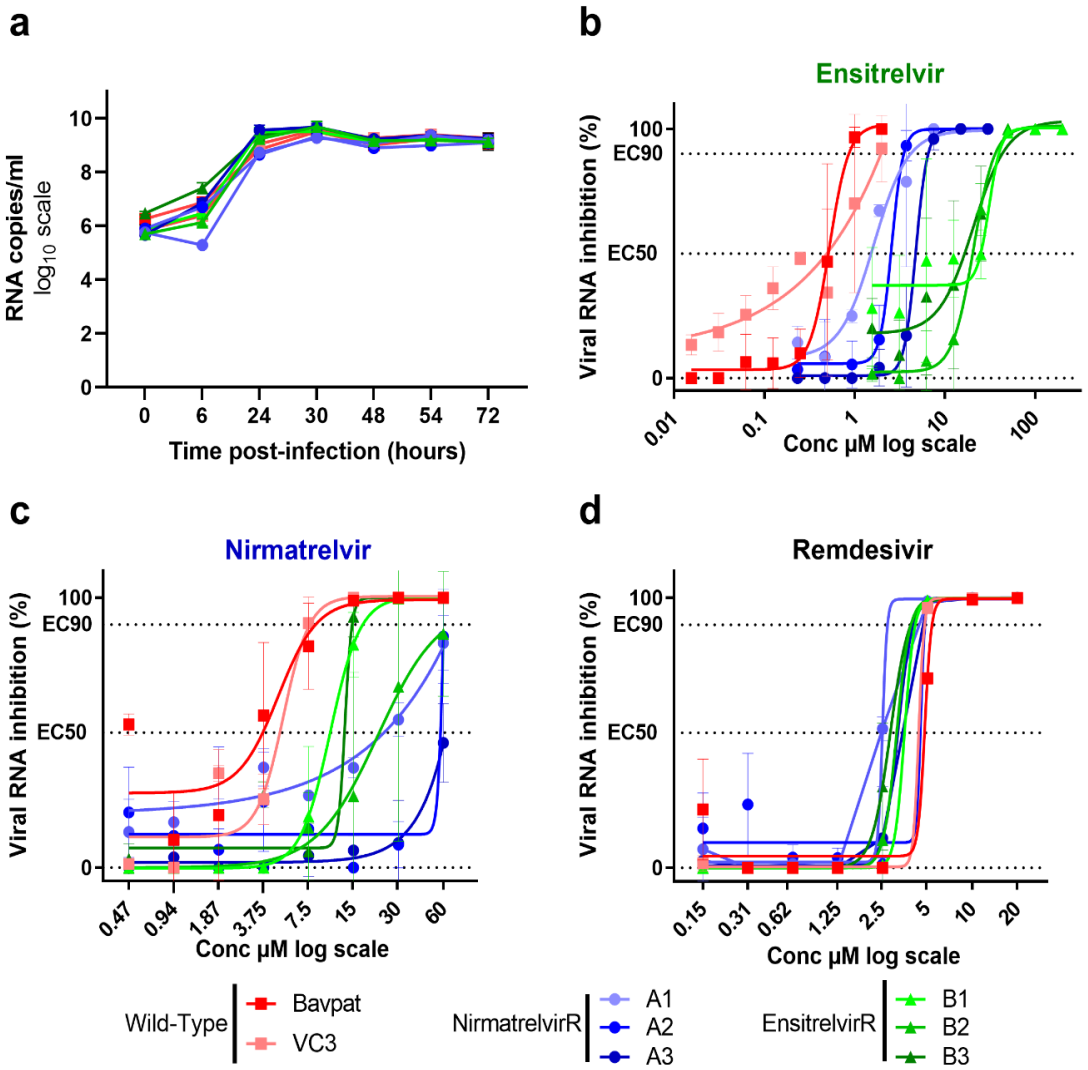

Figure 2: In vitro characterization of nirmatrelvir and ensitrelvir resistant strains.
a) Kinetics of replication in VeroE6 TMPRSS2 cells Data presented are from two technical replicates and error bars show mean±s.d ; Dose response curves reporting the susceptibility of SARS-CoV-2 mutants and two wild type strain against b) ensitrelvir c) nirmatrelvir and d) remdesivir. Data presented are from three technical replicates in VeroE6-TMPRSS2 cells, and error bars show mean±s.d

reduced sensitivity to nirmatrelvir (3 to 6-fold). On the other hand, the three nirmatrelvirR mutants showed a greater decreased in sensitivity (6 to 17-fold) (Fig. 2c Table 1). Interestingly, strains nirmatrelvirR-A2 and nirmatrelvirR-A3 showed the greatest resistance, despite having only one and two mutations, respectively. These results confirm that the T21I mutation and the combinations T21I-T304A and T21I-L50F-E166A do confer resistance to nirmatrelvir.

		Wild type		ensitrelvirR			nirmatrelvirR		
		Bavpat	VC3	B1	B2	B3	A1	A2	A3
nirmatrelvir	EC_{50} (µM)	3.7	4.8	10.5	22.3	13.1	24.0	57.5	62.2
	EC_{90} (µM)	8.4	7.6	17.3	69.5	14.7	>60	>60	>60
	Fold change	-	1.3	2.8	6.0	3.5	6.5	15.5	16.8
ensitrelvir	EC_{50} (µM)	0.5	0.5	25.0	20.3	22.7	1.5	2.5	4.8
	EC_{90} (µM)	0.9	2.0	39.6	36.1	37.0	4.2	3.5	6.6
	Fold change	-	1.0	49.0	39.9	44.5	3.0	5.0	9.3
remdesivir	EC_{50} (µM)	4.8	4.4	3.5	3.1	2.8	2.5	4.5	3.2
	EC_{90} (µM)	5.4	4.8	4.1	3.9	3.9	2.7	4.8	4.0
	Fold change	-	0.9	0.7	0.7	0.6	0.5	0.9	0.7

Table 1 : Activity of ensitrelvir, nirmatrelvir and remdesivir against wild type and mutants strains. Interpolated EC_{50} values are expressed in µM. Fold change reductions were calculated in comparison with the EC_{50} of the BavPat strain. F.c : fold change

f.c<5	5<f.c<10	10<f.c<100

Ensitrelvir is not efficacious against M49L ensitrelvir -resistant strain *in vivo*

Nirmatrelvir mutants have already been extensively studied(Iketani *et al*, 2023; Kiso *et al*, 2023a; Heilmann *et al*, 2022) but the ensitrelvir resistance mutation M49L has never been evaluated alone *in vivo*. To assess the ability of this mutationL to confer resistance to ensitrelvir *in vivo*, we used a hamster model of SARS-CoV-2 infection previously developed for antiviral evaluation(Driouich *et al*, 2021; Touret *et al*, 2021a; Driouich *et al*, 2022). We infected groups of 6 hamsters intranasally with either the wild type virus (BavPat), or M49L-R strain (B2). In addition to untreated groups, hamsters were administered 30 or 60 mg/kg of ensitrelvir orally twice a day. This regimen has previously been validated in two murine models(Unoh *et al*, 2022; Kiso *et al*, 2023b).
We observed that the M49L- ensitrlevirR strain and the wild type exhibited similar levels of replication in lungs of untreated hamster (no statistical differences) both in terms of viral RNA yield and infectious titers (Fig. 3 a and b). Regarding clinical follow-up, both the M49L-R strain and the wild-type induced a similar weight loss in hamsters (Fig. 3 c and d). These results show that, as observed *in vitro*, the selection process for resistance mutations has not deeply altered the replication characteristics and the pathogenicity of this strain in our model.
Regarding the antiviral effect of ensitrelvir on the wild-type strain, we observed a significant decrease in the amount of viral RNA and infectious titer in lungs, with a dose-response effect (Fig 3 a and b). Furthermore, animals treated with 60 mg/kg had a similar clinical follow-up to uninfected hamsters with no statistical differences in weight change, suggesting a beneficial effect of treatment on clinical outcome (Fig 3 c and Supplemental Fig.1). Animals treated with

30 mg/kg had an intermediate clinical follow-up between untreated infected hamsters and uninfected hamsters, with a similar trend to uninfected hamsters despite a decline between day 1 and 2 (Fig. 3 c and Supplemental Fig.1). These results indicate significant antiviral activity of ensitrelvir at both doses tested on the wild-type strain.

Regarding the antiviral effect of ensitrelvir on the resistant strain, we observed no significant decrease in viral RNA levels or infectious titers in lungs compared to control, regardless of the dosing regimen (Fig. 3 a and b). Furthermore, animals treated with 30 and 60 mg/kg had a clinical follow-up similar to untreated infected hamsters with no statistical differences in weight change to untreated infected hamsters, suggesting no beneficial effect of treatment on clinical outcome (Fig. 3d and Supplemental Fig.1). These results indicate a lack of efficacy of ensitrelvir at both doses tested on the mutant strain containing the M49L mutation in NSP5. This result is in line with that obtained with the M49L/E166A double mutant in the same hamster model(Kiso *et al*, 2023b), and demonstrates the ability of M49L to confer resistance to ensitrelvir even if in the absence of E166A.

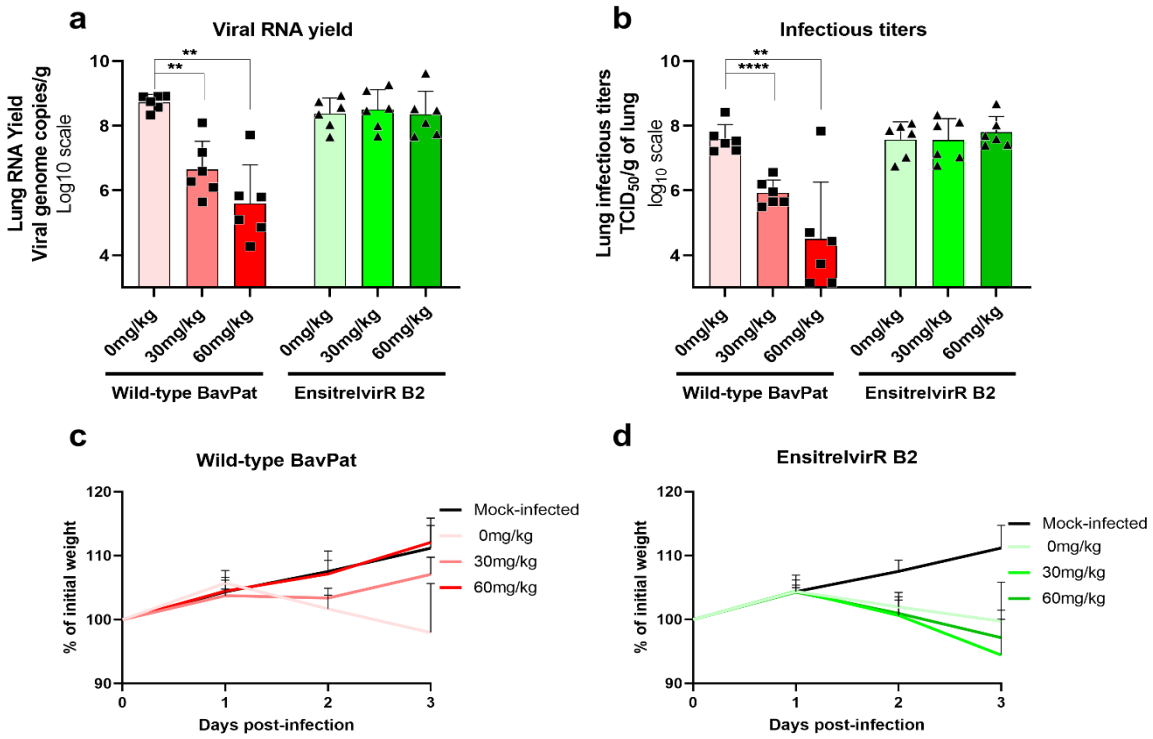

Figure 3: Antiviral activity of oral ensitrelvir treatment in a hamster model against wild type and resistant SARS-CoV-2 strains
Groups of 6 hamsters were intranasally infected with 104 TCID50 of virus. Animals received ensitrelvir orally twice a day at 0 (untreated group), 30 or 60 mg/kg. a) Viral replication in lung based on viral RNA yields (measured using an RT-qPCR assay) expressed in viral genome copies/g of lung. b) Viral replication in lung based on infectious titers (measured using a TCID50 assay) expressed in TCID50/g of lung. c-d) Clinical course of the disease (n=6 animals/group). Normalized weight at day n was calculated as follows: % of initial weight of the animal at day n. Data represent mean±SD. Two-sided statistical analysis was performed using Shapiro-Wilk normality test and Student t-test, ** and **** indicate and average significant value lower than that of the untreated group, with a p-value ranging between 0.001-0.01 and lower to 0.0001 respectively.

The M49L mutation prevalence increased over the last 6 months and has emerged in prominent lineages

The emergence of resistance mutations can drastically limit the use of the antiviral therapy affected. Resistance may emerge during prolonged use of the molecule in a patient with ongoing viral replication but can also occur naturally – without any specific selective pressure due to the use of the molecule in question. Our experiments show that the M49L mutation alone can confer resistance to ensitrelvir and previous reports have described M49L in circulating SARS-CoV-2 variants(Kawashima *et al*, 2023; Ip *et al*, 2023). The prevalence of this mutation in recent months and in particular, since the commercialization of ensitrelvir in Japan, has, however, not been reported.

We therefore searched on GISAID for all SARS-CoV-2 sequences carrying the M49L mutation. We found that, as of 30th of October 2023, only 267 (0.00165%) of the 16,167,749 SARS-CoV-2 sequences available on GISAID present an M to L amino acid substitution at position 49 in the NSP5 gene. Using sequence collection dates, we evaluated the distribution over time of all M49L-carrying SARS-CoV-2 sequences. We found that M49L was first reported on the 13th August 2020, and has been observed almost monthly since then (Figure 4a), with an apparent global prevalence of 0.00168% (total number of sequences with collection date on or after 13th August 2020: 15,929,475). When looking at the most recent time span, we found that more M49L-carrying sequences have been reported between May and October 2023 (count: 154; prevalence: 0.036%) than over the previous 21 months (count: 113 M49L; prevalence: 0.0007%). These numbers indicate that while M49L corresponds to a very small proportion of the sequences observed until today, its prevalence has increased during the last 6 months.

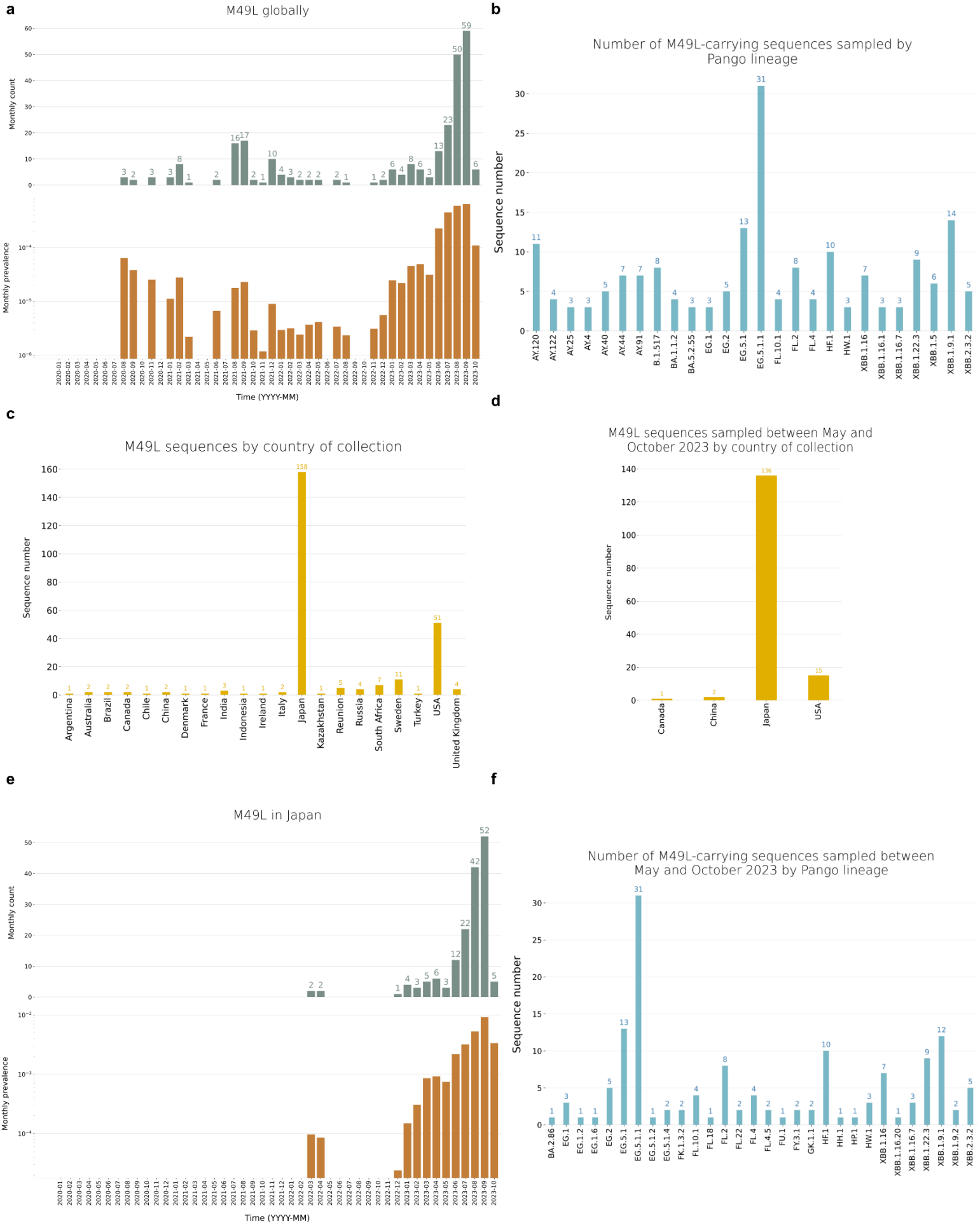

232

Figure 4 : M49L-carrying distribution in time, space, and across lineages. a) Global monthly counts (upper panel) and prevalences (lower panel) of M49L-sequences, based on all SARS-CoV-2 genomes publicly available on GISAID as of 2023-11-13. b) Number of M49L sequences observed by lineage, for each of the 30 Pango lineages most frequently observed among M49L sequences. c) Number of M49L sequences observed by country of collection. d) Number of M49L sequences observed by country of collection for sequences collected between May and October 2023. e) Monthly counts (upper panel) and prevalences (lower panel) of M49L-sequences in Japan, based on all SARS-CoV-2 genomes publicly available on GISAID as of 2023-11-13. f) Number of recent M49L sequences (collection date between October and May 2023) observed by lineage, for each of the 30 Pango lineages most frequently observed among recent M49L sequences.

The repeated observations of low numbers of M49L-carrying sequences since the first year of the pandemic suggest that the mutation has emerged on multiple occasions and in several SARS-CoV-2 lineages. We used the Pangolin online lineage assigner(O'Toole *et al*, 2021) to determine the Pango lineage of each of the 267 sequences with the M49L mutation. We found that M49L-carrying sequences are distributed across 90 different lineages, including Alpha, Delta, and Omicron, with up to 31 sequences belonging to the same lineage (Figure 4b, Supp. Table 1). The most prevalent lineages among M49L-carrying sequences are EG.5.1.1 (11.6%), XBB.1.9.1 (5.6%), and EG.5.1 (4.9%). These three lineages are "active" (last observed less than a year ago) and classified either as "variant of interest" (VOI) or as "variant under monitoring" (VUM) by the WHO(Tracking SARS-CoV-2 variants). Overall, these results indicate that NSP5 M49L can emerge in multiple genomic backgrounds and is present in active, currently prominent, lineages.

The recent increase in the prevalence of M49L appears to be linked to a specific selective pressure in Japan

Resistance against an antiviral therapy may occur naturally in circulating lineages but the use of a drug may favor the emergence of resistance mutations. Using the collection dates of M49L-carrying sequences, we showed that their proportion has been multiplied by more than 50 times in the last 6 months. Several scenarios may explain this increase in observation frequency: (i) a specific selective pressure; (ii) a more favorable genomic background; (iii) increased transmission.

The increased prevalence of the M49L resistance mutation observed in this study may be due to the existence of specific selective pressure, *i.e.* the use of the drug to which the compound confers resistance, ensitrelvir. The only country where this drug is used is Japan, where it first received an emergency use approval in November 2022, and was made commercially available in April 2023(Xocova to Be Commercially Available from March 31). When we evaluated the spatial distribution -in terms of country of origin- of M49L sequences, we found that Japan is by far the most important country of origin for M49L sequences, with 59.9% of sequences originating in Japan overall, a number that increases to 88.3% when considering only collection dates between May and October 2023 (Figure 4c-d). These results indicate that the vast majority of the M49L-carrying sequences collected over recent months originate from Japan.

When analyzing the time distribution of all M49L-sequences from Japan, we found that M49L has been observed only 4 times before December 2022 but almost monthly since then (Figure 4e), with especially high monthly prevalence values (above 0.2%) since June 2013. The timing of the increase in the prevalence of M49L and the origin of M49L sequences both align well with the use of Xocova® in Japan, suggesting that this selective pressure may favor the emergence of the mutation.

Another factor that may however, explain the recent increase in M49L sequences overall and in Japan more specifically, is the local circulation of lineages with a genomic background more favorable for the emergence of the mutation. To evaluate if recent M49L-sequences were associated with a specific genomic background, we analyzed their lineage distribution. We found that between May and October 2023, M49L occurred in 44 different lineages globally and in 40 different lineages in Japan including, EG.*, FL.*, GJ.*, HF.*, XBB.1.9.*, and XBB.1.16.*

lineages (Figure 4f). These results indicate that multiple distinct lineages can accommodate the M49L mutation.

When considering M49L-sequences from the most prevalent lineage, EG.5.1.1, 93.5% of them appear to originate in Japan, and only 3.2% both in the US and in Canada. Based on GISAID data, EG.5.1.1 appears to have circulated to levels on the same order of magnitude (or greater) to that observed over the last 6 months in Japan (7.6% of 37550 total sequences), in the US (3.8% of 146709 total sequences), in Canada (6.8% of 46555 total sequences), and in China (18.2% of 34404 total sequences). If the increase in M49L prevalence was driven by the genomic background of EG.5.1.1 being more favorable, this mutation would have also emerged more frequently in other locations where the lineage has established sustained transmission. These observations indicate that the recent increase in M49L prevalence is not driven by a single -or a few- more favorable genomic background.

Repeated emergence, rather than increased transmission, contributed to the recent increase in M49L prevalence

Another phenomenon that may have participated in increasing the prevalence of M49L in recent month is the formation of large transmission chains by naturally-occurring M49L mutant. The distribution of recent M49L sequences across 44 different lineages suggests that increased emergence events, rather than increased transmission, fueled the rise in M49L detections. However, the presence of a large transmission chain within the main lineage EG.5.1.1 may have been an exacerbating factor.

To determine whether recent M49L-carrying sequences from the most prominent lineage, EG.5.1.1, correspond to a single or multiple emergence events, we performed a phylogenetic inference based on a set of publicly available SARS-CoV-2 genomes. Using a maximum-likelihood approach, we inferred the phylogenetic relationships between all M49L-carrying EG.5.1.1 sequences and a set of EG.5.1.1 sequences collected between July and October in Japan and North America (to match the spatio-temporal distribution of the M49L genomes). In the resulting phylogeny, we identified 12 different M49L emergence events, associated either with single tips, or with entire well-supported clades encompassing up to 10 sequences (Figure 5). Our findings were broadly similar across 10 inference replicates. These results show

that recent M49L-carrying sequences do not form a single clade -- the mutation emerged at least on 12 independent occasions within that lineage.

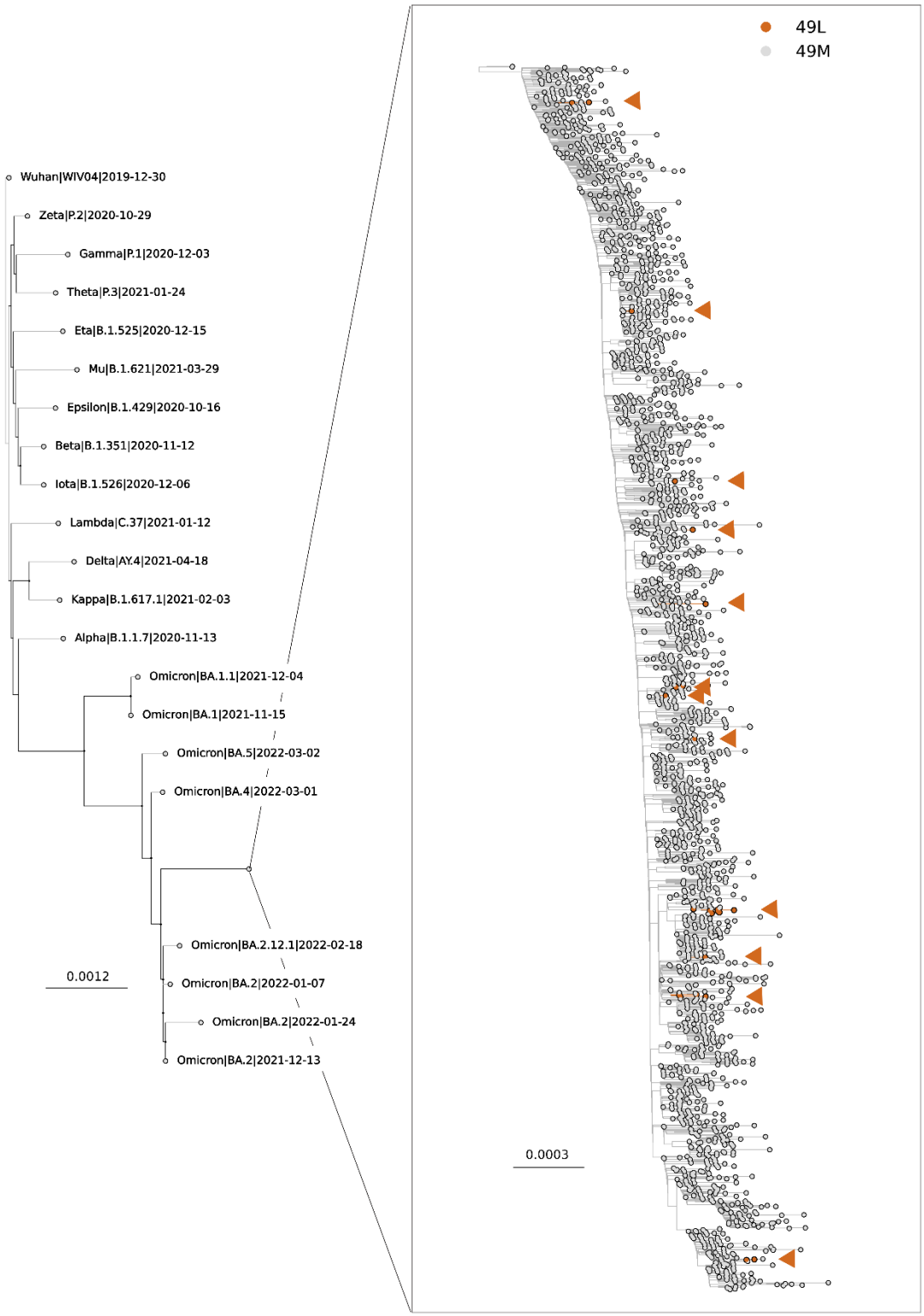

Figure 5: Maximum-likelihood phylogeny with a zoom on the EG.5.1.1 lineage. Branches and tips associated with M49L-carrying sequences are highlighted in orange. Orange arrows indicate M49L emergence events.

Discussion

In this study, we experimentally generated six viruses carrying resistance mutations to clinical stage SARS-CoV-2 protease inhibitors. We obtained three viruses with different sets of mutations for nirmatrelvir. For ensitrelvir, on the other hand, all three strains had the same mutation M49L. *In vitro* characterisation showed that nirmatrelvir-resistant strains had low resistance to ensitrelvir, but higher resistance to nirmatrelvir. Similarly, ensitrelvir-resistant strains showed low resistance to nirmatrelvir but much higher resistance to ensitrelvir. Finally, we investigated *in vivo* the resistance of an EnsitrelvirR M49L strain to two regimens of ensitrelvir and found that it completely escaped the inhibition induced by this antiviral compound.

We obtained resistance mutations after 16 passages with an increasing concentration of nirmatrelvir, which is similar to what has already been shown by Iketani and colleagues(Iketani *et al*, 2023). Indeed, these specific mutations have already been obtained using a similar approach: the T21I mutation was generated alone or in combination with E166V or T304I, exactly as in our study. This mutation, along with T304L, was predominantly acquired as initial mutation(Iketani *et al*, 2023). Interestingly, in the VeroE6 TMPRSS2 cell line, we obtained a mutation at residue 166, whereas in the study by Iketani and colleagues(Iketani *et al*, 2023) a mutation at this position only appeared in HUH.7 and not in VeroE6 , and the authors supposed that it was specific to this cell line. The mutation on residue 166 had already been described and was shown to reducer viral replicative fitness, but this fitness could be restored by the addition of the T21I mutation(Iketani *et al*, 2023). In our study, we confirmed this observation by showing that the replication capacity of our mutant (A1) carrying both T21I and E166A was the same as that of the wild type. Finally the mutation at residue 166 was the only one obtained in the substrate binding site; the others are situated at a distal position from nirmatrelvir predicted binding site (over 5 Å(Iketani *et al*, 2023)).

For ensitrelvir, we obtained three viruses with the same mutation, M49L. This mutation has already been obtained in a similar experiment, but with a shorter passage number(Kiso *et al*, 2023a). It is also present in circulating isolates of SARS-CoV-2(Kawashima *et al*, 2023; Noske *et al*, 2023; Moghadasi *et al*, 2023b). Visualization of the 3CLpro M49L complex with ensitrelvir shows that the greater hydrophobicity of isoleucine, compared to the methionine, caused the inhibitor to move to another site, which affects its antiviral activity(Noske *et al*, 2023).
We found *in vitro* moderate cross resistance between NirmatrelvirR strains and ensitrelvir, and the same for EnsitrelvirR strains and Nirmatrelvir, in accordance with previous studies(Iketani *et al*, 2023; Moghadasi *et al*, 2023b). This suggests that replacing one of the two compounds with the other could compensate for the emergence of a resistance mutation during treatment.

We observed the greatest loss in activity with the couple ensitrelvir/M49L with a ~40-fold reduction in susceptibility for our three ensitrelvirR strains. This mutation had already been tested, alone, in two distinct enzymatic assays(Moghadasi *et al*, 2023b, 2023a) and in a VSV based cleavage system(Moghadasi *et al*, 2023b), with observed fold change values of 21.4, 25.4 and 10 respectively. In the only previous study that explored the effect of this mutation with a replicative virus (a mutated Delta strain generated by reverse genetic(Kiso *et al*, 2023b)) M49L was associated with a 37.4 fold change in a focus reduction assay(Kiso *et al*, 2023a). This

365 result is perfectly in line with our observation with the same range of reduction despite the
366 use of a different variant backbone. The fact that we found the same effect for a single amino
367 acid mutation but with a different backbone not only confirms but reinforces our result.
368 In the abovementioned study, the authors only studied the *in vivo* antiviral resistance of the
369 M49L/166A mutation pair(Kiso *et al*, 2023b). Regarding the single mutation M49L they only
370 explored its impact on the *in vitro* replication fitness and the *in vivo* pathogenicity. We went a
371 step further and explored the effect of this single mutation on ensitrelvir sensitivity, using
372 both, the ensitrelvir dose referred to in the study above (60mg/kg twice daily)(Kiso *et al*,
373 2023b) and a lower dose as in the original S-217622/ensitrelvir article (30mg/kg twice
374 daily)(Unoh *et al*, 2022). When animals were infected with the ensitrelvirR strain, we observed
375 no antiviral activity for either of ensitrelvir dose regimen and, in contrast to what was
376 observed with the wild-type strain, no clinical improvement. This implies that the M49L
377 mutation can be solely responsible for *in vivo* resistance. The same result at the highest
378 regimen was observed *in vivo* with the double mutants M49L/E166A(Kiso *et al*, 2023b). The *in*
379 *vitro* fold change of this combination is almost 200(Kiso *et al*, 2023b). Our result implies that
380 a single mutation inducing a change in susceptibility of 40, *i.e.* five times lower, is enough to
381 make ensitrelvir treatment ineffective in our animal model.
382
383 In the current study, we detailed a recent increase in the prevalence of M49L-carrying
384 sequences, linked it to a specific region, Japan, and showed that thisincrease is concommittant
385 to the use of ensitrelvir in the country (emergency approval and then commercialization)
386 rather than with the emergence of a more favorable viral genomic background. These initial
387 results are concerning and warrant further investigation, especially as several countries are
388 currently considering the drug for emergency approval(Xocova Filed for Conditional Approval
389 in South Korea; Drugmaker Shionogi inks deal to market COVID pill in China). It is crucially
390 important to better characterize the conditions and frequency of emergence of the M49L
391 mutation in patients treated with ensitrelvir. If an increased risk of resistance emergence
392 during patient treatment is confirmed, genomic monitoring may allow to both optimize the
393 medical efficacy and prevent the spread of resistant strains. In the event of resistance, it would
394 still be possible to replace ensitrelvir with nirmatrelvir, given the low level of cross-resistance
395 between the two molecules. However, this would be difficult for patients who had received
396 ensitrelvir treatment in the first instance, due to a contraindication to ritonavir, which is
397 present in Paxlovid®, the pharmaceutical formulation of nirmatrelvir.
398 To evaluate the potential duration of transmission for EG.5.1.1 M49L-mutants, we calculated
399 minimum clade-durations for all M49L-clades by calculating the difference in time between
400 the earliest and latest sampling dates among sequences of a given clade. We found that clade-
401 duration could be up to 58 days for M49L clades belonging to the EG.5.1.1 lineage. This first
402 assessment however, is based on a small number of clades (3) and on a limited sampling of
403 the recent circulating diversity of SARS-CoV-2. For computational tractability reasons we
404 focused our phylogenetic analysis on sequences from a single lineage (EG.5.1.1), specific
405 countries (Japan, North America), and subsampled our dataset. We believe that it is of the
406 utmost importance to pursue these investigations and to continue to monitor the ability of
407 M49L-carrying lineages to establish sustained transmission and to assess the risk of fixation of
408 the mutation.
409
410 Finally, while the use of ensitrelvir is probably linked to the emergence of M49L in recent
411 months in Japan, it is unlikely that 107 early sequences carrying M49L (identified between

August 2020 and October 2023) are linked to the use of this drug. The spontaneous circulation of strains carrying M49L may be a factor facilitating the emergence of resistance to ensitrelvir. This argues in favor of genetic monitoring of circulating strains to ensure that the treatments administered retain their full effectiveness. In addition, the range of antiviral treatments available against SARS-CoV-2 has become worryingly limited, with most commercial monoclonal drugs losing their activity against the most recent variants. Obviously, there is still a need to develop other antivirals targeting other viral proteins to broaden the therapeutic armory, and possibly to develop dual therapies as has been done for other viral diseases.

Author Contributions

Conceptualization : AN, FE, IS, EC and FT
Methodology :, JSD, AN, and FT
Formal analysis : SHB, JSD, RK, OB,GP,RA and FT
Investigation : SHB, JSD,RK, GP ,RA, OBand FT
Resources : XdL, FT and AN
Writing original draft: SHB, JSD, AN and FT;
Writing review & editing : all co-authors
Visualization SHB, JSD, RK, OB, AN and FT
Funding acquisition LF, CM, EC, XdL, AN and FT.

Acknowledgments

We thank Magali Gilles (UVE; Marseille), Gregory Moureau (UVE; Marseille) and Camille Placidi (UVE; Marseille) for their valuable technical contribution. We thank Edyth Parker for her recommendations on SARS-CoV-2 phylogenetic inference. We thank Pr. Drosten for providing the SARSCoV-2 strain through the European Research infrastructure EVA GLOBAL.
This work was by European Virus Archive Global (EVA GLOBAL) funded by the European Union's Horizon 2020 research and innovation program under grant agreement No. 871029 and by DNDi under support by the Wellcome Trust Grant ref: 222489/Z/21/Z through the COVID-19 Therapeutics Accelerator. Part of the work was done on the Aix Marseille University antivirals platform “AD2P”.

Declaration of interests

The authors declare that there have no conflict of interest.

Materials & Correspondence

Correspondence to Franck Touret (franck.touret@univ-amu.fr)

Supplemental Data

Supplemental figure 1: Clinical follow up after Wild-type (Bavpat) and EnsitrelvirR B2 SARS-CoV-2 viral challenge
A-B : Weight change at day 2 and at day 3 post infection in percentage, normalized to the body weight at day 0 of B.1 (G614) infection. C-D : Weight change at day 2 and at day 3 post infection in percentage, normalized to the body weight at day 0 of EnsitelvirR B2 infection. Bars represent means ± SD. The data were analyzed with the unpaired t test (fig.A-C) and Mann-Whitney test (fig B-D). *P < .05, **P < .01, ***P < .001.

Supplementary Table 1: Accession IDs, collection dates, submission dates, collection location, and Pango lineage (assigned using Pangolin lineage assigner) for all M49L sequences analyzed in this study.

Supplementary Table 2: GISAID accession IDs for all SARS-CoV-2 genomes (and attached metadata) analyzed in this study.

References

Beigel JH, Tomashek KM, Dodd LE, Mehta AK, Zingman BS, Kalil AC, Hohmann E, Chu HY, Luetkemeyer A, Kline S, *et al* (2020) Remdesivir for the Treatment of Covid-19 — Final Report. *New England Journal of Medicine* 383: 1813–1826

Bloom JD, Gong LI & Baltimore D (2010) Permissive Secondary Mutations Enable the Evolution of Influenza Oseltamivir Resistance. *Science* 328: 1272–1275

Driouich J-S, Cochin M, Lingas G, Moureau G, Touret F, Petit P-R, Piorkowski G, Barthélémy K, Laprie C, Coutard B, *et al* (2021) Favipiravir antiviral efficacy against SARS-CoV-2 in a hamster model. *Nat Commun* 12: 1735

Driouich J-S, Cochin M, Touret F, Petit P-R, Gilles M, Moureau G, Barthélémy K, Laprie C, Wattanakul T, Chotsiri P, *et al* (2022) Pre-clinical evaluation of antiviral activity of nitazoxanide against SARS-CoV-2. *eBioMedicine* 82: 104148

Drugmaker Shionogi inks deal to market COVID pill in China *Nikkei Asia*

Hammond J, Leister-Tebbe H, Gardner A, Abreu P, Bao W, Wisemandle W, Baniecki M, Hendrick VM, Damle B, Simón-Campos A, *et al* (2022) Oral Nirmatrelvir for High-Risk, Nonhospitalized Adults with Covid-19. *New England Journal of Medicine* 386: 1397–1408

Heilmann E, Costacurta F, Moghadasi SA, Ye C, Pavan M, Bassani D, Volland A, Ascher C, Weiss AKH, Bante D, *et al* (2022) SARS-CoV-2 3CLpro mutations selected in a VSV-based system confer resistance to nirmatrelvir, ensitrelvir, and GC376. *Science Translational Medicine* 15: eabq7360

Hoertel N, Boulware DR, Sánchez-Rico M, Burgun A & Limosin F (2022) Prevalence of Contraindications to Nirmatrelvir-Ritonavir Among Hospitalized Patients With COVID-19 at Risk for Progression to Severe Disease. *JAMA Network Open* 5: e2242140

Hunter JD (2007) Matplotlib: A 2D Graphics Environment. *Computing in Science & Engineering* 9: 90–95

Iketani S, Mohri H, Culbertson B, Hong SJ, Duan Y, Luck MI, Annavajhala MK, Guo Y, Sheng Z, Uhlemann A-C, *et al* (2023) Multiple pathways for SARS-CoV-2 resistance to nirmatrelvir. *Nature* 613: 558–564

Imai M, Ito M, Kiso M, Yamayoshi S, Uraki R, Fukushi S, Watanabe S, Suzuki T, Maeda K, Sakai-Tagawa Y, *et al* (2022) Efficacy of Antiviral Agents against Omicron Subvariants BQ.1.1 and XBB. *New England Journal of Medicine* 0: null

Ip JD, Wing-Ho Chu A, Chan W-M, Cheuk-Ying Leung R, Umer Abdullah SM, Sun Y & To KK-W (2023) Global prevalence of SARS-CoV-2 3CL protease mutations associated with nirmatrelvir or ensitrelvir resistance. *eBioMedicine* 91: 104559

Issues with SARS-CoV-2 sequencing data - SARS-CoV-2 coronavirus / nCoV-2019 Genomic Epidemiology (2020) *Virological*

500 Jin Z, Du X, Xu Y, Deng Y, Liu M, Zhao Y, Zhang B, Li X, Zhang L, Peng C, *et al* (2020) Structure of Mpro from
501 SARS-CoV-2 and discovery of its inhibitors. *Nature* 582: 289–293

502 Katoh K & Standley DM (2013) MAFFT Multiple Sequence Alignment Software Version 7: Improvements in
503 Performance and Usability. *Molecular Biology and Evolution* 30: 772–780

504 Kawashima S, Matsui Y, Adachi T, Morikawa Y, Inoue K, Takebayashi S, Nobori H, Rokushima M, Tachibana Y &
505 Kato T (2023) Ensitrelvir is effective against SARS-CoV-2 3CL protease mutants circulating globally.
506 *Biochem Biophys Res Commun* 645: 132–136

507 Kiso M, Furusawa Y, Uraki R, Imai M, Yamayoshi S & Kawaoka Y (2023a) In vitro and in vivo characterization of
508 SARS-CoV-2 strains resistant to nirmatrelvir. *Nat Commun* 14: 3952

509 Kiso M, Yamayoshi S, Iida S, Furusawa Y, Hirata Y, Uraki R, Imai M, Suzuki T & Kawaoka Y (2023b) In vitro and in
510 vivo characterization of SARS-CoV-2 resistance to ensitrelvir. *Nat Commun* 14: 4231

511 Korber B, Fischer WM, Gnanakaran S, Yoon H, Theiler J, Abfalterer W, Hengartner N, Giorgi EE, Bhattacharya T,
512 Foley B, *et al* (2020) Tracking Changes in SARS-CoV-2 Spike: Evidence that D614G Increases Infectivity
513 of the COVID-19 Virus. *Cell* 182: 812-827.e19

514 Minh BQ, Nguyen MAT & von Haeseler A (2013) Ultrafast Approximation for Phylogenetic Bootstrap. *Molecular*
515 *Biology and Evolution* 30: 1188–1195

516 Minh BQ, Schmidt HA, Chernomor O, Schrempf D, Woodhams MD, von Haeseler A & Lanfear R (2020) IQ-TREE
517 2: New Models and Efficient Methods for Phylogenetic Inference in the Genomic Era. *Molecular*
518 *Biology and Evolution* 37: 1530–1534

519 Moghadasi SA, Biswas RG, Harki DA & Harris RS (2023a) Rapid resistance profiling of SARS-CoV-2 protease
520 inhibitors. *npj Antimicrob Resist* 1: 1–4

521 Moghadasi SA, Heilmann E, Khalil AM, Nnabuife C, Kearns FL, Ye C, Moraes SN, Costacurta F, Esler MA, Aihara
522 H, *et al* (2023b) Transmissible SARS-CoV-2 variants with resistance to clinical protease inhibitors.
523 *SCIENCE ADVANCES*

524 Noske GD, Silva E de S, Godoy MO de, Dolci I, Fernandes RS, Guido RVC, Sjö P, Oliva G & Godoy AS (2023)
525 Structural basis of nirmatrelvir and ensitrelvir activity against naturally occurring polymorphisms of the
526 SARS-CoV-2 main protease. *Journal of Biological Chemistry* 299

527 O'Toole Á, Scher E, Underwood A, Jackson B, Hill V, McCrone JT, Colquhoun R, Ruis C, Abu-Dahab K, Taylor B, *et*
528 *al* (2021) Assignment of epidemiological lineages in an emerging pandemic using the pangolin tool.
529 *Virus Evol* 7: veab064

530 Owen DR, Allerton CMN, Anderson AS, Aschenbrenner L, Avery M, Berritt S, Boras B, Cardin RD, Carlo A,
531 Coffman KJ, *et al* (2021) An oral SARS-CoV-2 Mpro inhibitor clinical candidate for the treatment of
532 COVID-19. *Science* 374: 1586–1593

533 Pinto D, Park Y-J, Beltramello M, Walls AC, Tortorici MA, Bianchi S, Jaconi S, Culap K, Zatta F, De Marco A, *et al*
534 (2020) Cross-neutralization of SARS-CoV-2 by a human monoclonal SARS-CoV antibody. *Nature* 583:
535 290–295

536 REED LJ & MUENCH H (1938) A SIMPLE METHOD OF ESTIMATING FIFTY PER CENT ENDPOINTS12. *American*
537 *Journal of Epidemiology* 27: 493–497

538 Rockett R, Basile K, Maddocks S, Fong W, Agius JE, Johnson-Mackinnon J, Arnott A, Chandra S, Gall M, Draper J,
539 *et al* (2022) Resistance Mutations in SARS-CoV-2 Delta Variant after Sotrovimab Use. *N Engl J Med* 386:
540 1477–1479

541 Sasaki M, Tabata K, Kishimoto M, Itakura Y, Kobayashi H, Ariizumi T, Uemura K, Toba S, Kusakabe S, Maruyama
542 Y, *et al* (2022) S-217622, a SARS-CoV-2 main protease inhibitor, decreases viral load and ameliorates
543 COVID-19 severity in hamsters. *Science Translational Medicine* 15: eabq4064

544 Shionogi (2023) A Phase 3, Multicenter, Randomized, Double-Blind, 24-Week Study of the Clinical and Antiviral
545 Effect of S-217622 Compared With Placebo in Non-Hospitalized Participants With COVID-19
546 clinicaltrials.gov

547 Starr TN, Czudnochowski N, Liu Z, Zatta F, Park Y-J, Addetia A, Pinto D, Beltramello M, Hernandez P, Greaney AJ,
548 *et al* (2021) SARS-CoV-2 RBD antibodies that maximize breadth and resistance to escape. *Nature* 597:
549 97–102

550 Takashita E, Kinoshita N, Yamayoshi S, Sakai-Tagawa Y, Fujisaki S, Ito M, Iwatsuki-Horimoto K, Halfmann P,
551 Watanabe S, Maeda K, *et al* (2022) Efficacy of Antiviral Agents against the SARS-CoV-2 Omicron
552 Subvariant BA.2. *N Engl J Med* 386: 1475–1477

553 Touret F, Baronti C, Bouzidi HS & de Lamballerie X (2022) In vitro evaluation of therapeutic antibodies against a
554 SARS-CoV-2 Omicron B.1.1.529 isolate. *Sci Rep* 12: 4683

555 Touret F, Baronti C, Goethals O, Van Loock M, de Lamballerie X & Querat G (2019) Phylogenetically based
556 establishment of a dengue virus panel, representing all available genotypes, as a tool in dengue drug
557 discovery. *Antiviral Res* 168: 109–113

558 Touret F, Driouich J-S, Cochin M, Petit PR, Gilles M, Barthélémy K, Moureau G, Mahon F-X, Malvy D, Solas C, *et*
559 *al* (2021a) Preclinical evaluation of Imatinib does not support its use as an antiviral drug against SARS-
560 CoV-2. *Antiviral Res* 193: 105137

561 Touret F, Driouich J-S, Cochin M, Petit PR, Gilles M, Barthélémy K, Moureau G, Mahon F-X, Malvy D, Solas C, *et*
562 *al* (2021b) Preclinical evaluation of Imatinib does not support its use as an antiviral drug against SARS-
563 CoV-2. *Antiviral Research* 193: 105137

564 Touret F, Gilles M, Barral K, Nougairède A, van Helden J, Decroly E, de Lamballerie X & Coutard B (2020a) In
565 vitro screening of a FDA approved chemical library reveals potential inhibitors of SARS-CoV-2
566 replication. *Scientific Reports* 10: 13093

567 Touret F, Gilles M, Barral K, Nougairède A, van Helden J, Decroly E, de Lamballerie X & Coutard B (2020b) In
568 vitro screening of a FDA approved chemical library reveals potential inhibitors of SARS-CoV-2
569 replication. *Sci Rep* 10: 13093

570 Touret F, Giraud E, Bourret J, Donati F, Tran-Rajau J, Chiaravalli J, Lemoine F, Agou F, Simon-Lorière E, van der
571 Werf S, *et al* (2023) Enhanced neutralization escape to therapeutic monoclonal antibodies by SARS-
572 CoV-2 omicron sub-lineages. *iScience* 26: 106413

573 Tracking SARS-CoV-2 variants

574 University of Minnesota (2023) Strategies and Treatments for Respiratory Infections &Amp; Viral Emergencies
575 (STRIVE): Shionogi Protease Inhibitor clinicaltrials.gov

576 Unoh Y, Uehara S, Nakahara K, Nobori H, Yamatsu Y, Yamamoto S, Maruyama Y, Taoda Y, Kasamatsu K, Suto T,
577 *et al* (2022) Discovery of S-217622, a Noncovalent Oral SARS-CoV-2 3CL Protease Inhibitor Clinical
578 Candidate for Treating COVID-19. *J Med Chem* 65: 6499–6512

579 Vangeel L, Chiu W, De Jonghe S, Maes P, Slechten B, Raymenants J, André E, Leyssen P, Neyts J & Jochmans D
580 (2022) Remdesivir, Molnupiravir and Nirmatrelvir remain active against SARS-CoV-2 Omicron and
581 other variants of concern. *Antiviral Res* 198: 105252

582 Wang M, Cao R, Zhang L, Yang X, Liu J, Xu M, Shi Z, Hu Z, Zhong W & Xiao G (2020) Remdesivir and chloroquine
583 effectively inhibit the recently emerged novel coronavirus (2019-nCoV) in vitro. *Cell Research*: 1–3

584 Williamson BN, Feldmann F, Schwarz B, Meade-White K, Porter DP, Schulz J, van Doremalen N, Leighton I, Yinda
585 CK, Pérez-Pérez L, *et al* (2020) Clinical benefit of remdesivir in rhesus macaques infected with SARS-
586 CoV-2. *Nature* 585: 273–276

587 Xocova Filed for Conditional Approval in South Korea *PHARMA JAPAN*

588 Xocova to Be Commercially Available from March 31 *PHARMA JAPAN*

589

590 Materiel and methods

591 Experimental model

592 ***Cell line***

593 VeroE6/TMPRSS2 cells (ID 100978) were obtained from CFAR and were grown in MEM
594 (Minimal Essential Medium-Life Technologies) with 7 .5% heat-inactivated Fetal Calf Serum
595 (FCS; Life Technologies with 1% penicillin/streptomycin PS, 5000U.mL^{-1} and 5000µg.mL^{-1}
596 respectively (Life Technologies) and supplemented with 1% non-essential amino acids (Life
597 Technologies) and G-418 (Life Technologies), at 37°C with 5% CO_2.
598

599 ***Viral strain***

600 SARS-CoV-2 strain BavPat1 was obtained from Pr. C. Drosten through EVA GLOBAL
601 (https://www.european-virus-archive.com/) and contains the D614G mutation.
602

603 ***Organisms/strains***

604 Three-week-old female Syrian hamsters (Mesocricetus auratus) were purchased from Janvier
605 labs. Three-week-old Syrian hamsters (Janvier labs) were maintained in ISOcage P -
606 Bioexclusion System (Techniplast) with unlimited access to water/food and 14h/10h
607 light/dark cycle. Animals were monitored and weighed daily throughout the duration of the
608 study to detect the appearance of any clinical signs of illness/suffering.
609

610 *Antiviral Compounds*

611 Remdesivir was purchased from BLDpharm. ensitrelvir and nirmatrelvir were purchased
612 from MedChemexpress
613
614

615 Method details

616

617 RNA extraction and quantification

618 Viral RNA was extracted from 100 µL of cell supernatant from passages P8 and P16 using a
619 QIAamp Viral RNA kit on the automated QIAcube (Qiagen), following the manufacturer's
620 instructions. Relative quantification of viral RNA was performed using the GoTaq® 1-Step RT-qPCR
621 System kit (Promega). The mixture contained 5 µL of 2x Master Mix, 0.25 µL of each primer (250 nM),
622 0.07 µL of probe (75 nM), 0.2 µL of GoScript RT Mix and 3.8 µL of extracted nucleic acids. Assays were
623 performed using the QuantStudio 12 K Flex real-time PCR machine (Life technologies) under the
624 following conditions : 50°C for 15 min, 95°C for 2 min, followed by 40 cycles of 95°C for 3 s, 60°C for 30

625 s. Data collection took place during the 60°C step. Synthetic RNA was used to calculate the amount of
626 viral RNA from standard curves.
627

628 EC_{50} determination

629 One day prior to infection, 5×10^4 VeroE6/TMPRSS2 cells per well were seeded in 100µL assay medium
630 (containing 2.5% FBS) in 96 well culture plates.The next day, antiviral compounds were added using
631 the D300e dispenser (TECAN) with eight ½ dilutions . Then, 50 µL/well of a virus mix diluted in medium
632 was added to the wells. Each well was inoculated with 100 $TCID_{50}$ of virus which correspond here to a
633 MOI at 0.002 as classically used for SARS-CoV-2(Touret *et al*, 2020b). Prior to the assay it was verified
634 for each variant that with this MOI, viruses in the cell culture supernatants were harvested during the
635 logarithmic growth phase of viral replication at 48 hours post infection (Touret *et al*, 2019, 2022) . Four
636 virus control wells were included within the plate.Quantification of the viral genome by real-time RT-
637 qPCR as previously described (Touret *et al*, 2020a).Nucleic acid from 100µL of cell supernatant were
638 extracted using QIAamp 96 DNA kit and Qiacube HT robot (both from Qiagen). Viral RNA was quantified
639 by real-time RT-qPCR (GoTaq 1 step RT-qPCR kit, Promega). Quantification was provided by serial
640 dilutions of an appropriate T7-generated synthetic RNA standard. RT-qPCR reactions were performed
641 on QuantStudio 12K Flex Real-Time PCR System (Applied Biosystems) and analyzed using QuantStudio
642 12K Flex Applied Biosystems software v1.2.3. Primers and probe sequences, which target SARS-CoV-2
643 N gene, were: Fw: 5'-GGCCGCAAATTGCACAAT-3' ; Rev : 5'-CCAATGCGCGACATTCC-3'; Probe: 5'-FAM-
644 CCCCCAGCGCTTCAGCGTTCT-BHQ1-3'. Viral inhibition was calculated as follow: 100* (quantity mean
645 VC- sample quantity)/ quantity mean VC. The 50% effective concentrations (EC50 compound
646 concentration required to inhibit viral RNA replication by 50%) were determined using logarithmic
647 interpolation after performing a nonlinear regression (log(agonist) vs. response --Variable slope (four
648 parameters)) as previously described (Touret *et al*, 2019, 2022, 2021b). All data obtained were
649 analyzed using GraphPad Prism 9 software (Graphpad software).
650

651 Viral titration

652 One day prior to infection, 5×10^4 VeroE6 cells per well were seeded in 100µL assay medium (containing
653 2.5% FBS) in 96 well culture plates.Virus titration was performed using 96-well culture plates
654 containing confluent VeroE6 cells inoculated with 150µL per well of four-fold dilutions of samples
655 (dilution with medium supplemented with 2.5% FBS)Plates were incubate 6 days (37°C, 5% CO2) The
656 absence or presence of cytopathic effect in each well was read.Infectious titers were estimated using
657 the Reed & Muench method (REED & MUENCH, 1938).
658

659 Mutants Generation

660 One day prior to infection, 5×10^5 VeroE6/TMPRSS2 cells per well were seeded in 2mL assay medium
661 (containing 2.5% FBS) in 12 well culture plates.The EC50s of Nirmatrelvir and Ensitrelvir were
662 determined as previously described.Once the EC50s of these two molecules had been determined,
663 successive passages of the virus at an MOI of 0.01 with increasing concentrations of these molecules
664 were carried out in triplicate. Two passages at the EC50 concentration, two passages at 2x [EC50], two
665 passages at 4 x [EC_{50}] and ten passages at 8 x [EC_{50}]. A no-molecule control was also run in triplicate.
666 Between each run, the plates were incubated at 37°C/5% CO2 for 72 h. We performed extraction with
667 Qiagen's EZ1 automated system and NGS sequencing (Ion Torrent) for passages P8 and P16. We then
668 performed viral production for passage P16. Viral titration by $TCID_{50}$/mL and growth kinetics of all P16
669 viruses were performed.
670
671

672 Growth kinetics

673 One day prior to infection, 5×10^6 VeroE6/TMPRSS2 cells per well were seeded in 3mL assay medium
674 (containing 2.5% FBS) in 6 well culture plates. The following day, the wells were infected with each

675 virus with MOI 0.01, in 1mL of medium (containing 2.5% FBS), and incubated at 37°C/5% Co2 for 2h.
676 Sampling at 0h took place before incubation. The experiment was performed in duplicate. After
677 incubation, a wash with HBSS was performed and 3mL of medium (containing 2.5% FBS) was added to
678 each well. Samples were taken at 6h pi, 24h pi, 30h pi, 48h pi, 54h pi and 72h pi. They were extracted
679 by Qiacube as described above and qRT performed.
680

681 Animal experiments

682 In vivo experiments were approved by the local ethical committee (C2EA—14) and the French
683 "Ministère de l'Enseignement Supérieur, de la Recherche et de l'Innovation" (APAFIS#23975). All
684 experiments were conducted in BSL 3 laboratory.
685 Three-week-old Syrian hamsters (Janvier labs) were maintained in ISOcage P - Bioexclusion System
686 (Techniplast) with unlimited access to water/food and 14h/10h light/dark cycle. Animals were
687 monitored and weighed daily throughout the duration of the study to detect the appearance of any
688 clinical signs of illness/suffering. Groups of animals were intranasally infected under general anesthesia
689 (isofluorane) with 50µL containing $2x10^4$ TCID50 of virus diluted in 0.9% sodium chloride solution.
690 Animal were treated via oral route two times a day with 30 or 60 mg/kg of Ensitrelvir suspended in 0.5
691 % methylcellulose
692 Nasal washes were performed under general anesthesia (isoflurane). Blood and organs were collected
693 immediately after euthanasia (cervical dislocation; realized under general anesthesia (isofluorane)).
694 Nasal washes were performed with 150µl 0.9% sodium chloride solution which was transferred into
695 1.5mL tubes containing 0.5mL of 0.9% sodium chloride solution, then centrifuged at 16,200g for 10
696 minutes and stored at -80°C. Left pulmonary lobes were washed in 10mL of 0.9% sodium chloride
697 solution, blotted with filter paper, weighed and then transferred into 2mL tubes containing 1mL of
698 0.9% sodium chloride solution and 3mm glass beads. They were then crushed using a Tissue Lyser
699 machine (Retsch MM400) for 20min at 30 cycles/s and centrifuged 10 min at 16,200g. Supernatant
700 media were transferred into 1.5mL tubes, centrifuged 10 min at 16,200g and stored at -80°C.
701 Right apical lobes were collected into 2mL tubes containing 0.75mL of Qiazol lysis reagent (Qiagen)
702 and 3mm glass beads. They were then crushed using a Tissue Lyser machine (Retsch MM400) for 10min
703 at 30 cycles/s and stored at -80°C.
704

705 Sequence analysis of the full-length genome

706 200µL of lung of infectious cell supernatant (virus stock and HAE) was inactivated with an equal volume
707 of VXL lysis buffer (Qiagen) and viral RNA was extracted using an EZ1 Advanced XL robot with the EZ1
708 mini virus 2.0 kit (both from Qiagen) and linear acrylamide (ThermoFisher Scientific) in place of carrier
709 RNA. The extracts were then subjected to quantitative real-time RT-PCR in order to standardize the
710 amounts of viral RNA used during complete genome amplification (see below).
711 A specific set of primers (Table XXX) was used to generate thirteen amplicons covering the entire
712 genome with the Superscript IV one step RT-PCR System (ThermoFisher Scientific). PCR mixes (final
713 volume 25µL) contained 2.5µL containing a standard quantity of viral RNA from the nucleic acid extract,
714 0.75µL of each primer (10µM), 12.5 µL of 2X Platinum SuperFi RT-PCR Master Mix, 8.25µL of RNA free
715 water and 0.25µL SuperScript IV RT Mix. Amplifications were performed with the following conditions:
716 15 sec at 55°C, 2 min at 98°C, then 40 cycles of 10 sec at 98°C, 10 sec à 56°C and 1.5 min at 72°C. Size
717 of PCR products was verified by gel electrophoresis. For each sample, an equimolar pool of all
718 amplicons was prepared and purified using Monarch PCR & DNA Cleanup Kit (New England Biolabs).
719 After Qubit quantification using Qubit® dsDNA HS Assay Kit and Qubit 2.0 fluorometer (Thermo
720 Fisher) amplicons were sonicated (Bioruptor®, Diagenode, Liège, Belgium) into 250pb long fragments.
721 Libraries were built adding to fragmented DNA barcode for sample identification and primers with Ion
722 Plus Fragment Library Kit using AB Library Builder System (Thermo Fisher). To pool equimolarly the
723 barcoded samples, a real time PCR quantification step was performed using Ion Library TaqMan™
724 Quantitation Kit (Thermo Fisher). Next steps included an emulsion PCR of the pools and loading on 530
725 chips performed using the automated Ion Chef instrument (Thermo Fisher), followed by sequencing

using the S5 Ion torrent technology (Thermo Fisher), following manufacturer's instructions. Consensus sequence was obtained after trimming of reads (reads with quality score <0.99, and length <100pb were removed and the 30 first and 30 last nucleotides were removed from the reads) and mapping of the reads on a reference (MT594401.1) using CLC genomics workbench software v.21.0.5 (Qiagen). Parameters for reference-based assembly consisted of match score = 1, mismatch cost = 2, length fraction = 0.5, similarity fraction = 0.8, insertion cost = 3, and deletion cost = 3. A de novo contig was also produced to ensure that the consensus sequence was not affected by the reference sequence. Mutation frequency for each position was calculated as the number of reads with a mutation compared to the consensus sequence divided by the total number of reads at that site.

Public sequence data analysis

Datasets

We downloaded all three sets of SARS-CoV-2 sequence from the GISAID public database: (1) all sequences (and attached metadata) containing an M to L change at position 49 in the NSP5 ; (2) all EG.5.1.1 sequences (filtering out low coverage and incomplete sequences) from Japan collected between July and October 2023 ; (3) all EG.5.1.1 sequences (filtering out low coverage and incomplete sequences) from North America collected between July and October 2023.

We first removed all sequences with >5% of ambiguous nucleotides from all datasets except for the one corresponding to EG.5.1.1 M49L sequence. Then, to obtain a computationally tractable dataset for phylogenetic inference, we randomly downsampled the EG.5.1.1 North America dataset (filtering out duplicates) to 500 sequences, and combined it with all EG.5.1.1 sequences from Japan. We added all EG.5.1.1 sequences carrying the M49L mutation. After the first maximum likelihood (ML) inference, we removed three sequences corresponding to extremely long terminal branches (GISAID Accession IDs: 18434659, 18226914, 18432517), yielding a final dataset of 2603 sequences. All GISAID accession numbers are available in Supp. Table 2, the alignment and trees are available at https://github.com/rklitting/SARS-CoV-2-resistance.

Phylogenetic analysis

For the M49L-sequences lineage analysis, we assigned lineages to each of the M49L sequences using the Pangolin lineage assigner (version 4.3)(O'Toole *et al*, 2021) . Classification failed for 3 out of the 267 sequences submitted (See Supp. Table 1).

For phylogenetic inference, we aligned the final EG.5.1.1 dataset to the reference genome WIV04 (GISAID Accession: 402124) using MAFFTv7(Katoh & Standley, 2013) . To provide some phylogenetic context to the EG.5.1.1 lineage, we added the set of genomes corresponding to WHO reference strains for VOCs, VUIs and VUMs provided by the Los Alamos national laboratory(Korber *et al*, 2020) .Finally, we performed the masking of sites previously identified as potential sequencing errors or suspect homoplasies(Issues with SARS-CoV-2 sequencing data - SARS-CoV-2 coronavirus / nCoV-2019 Genomic Epidemiology, 2020), and removed the 5' and 3' UTRs. We inferred a first ML phylogeny for this dataset using IQTREE2 under ModelFinder with ultrafast bootstrap approximation (1000 replicates)(Minh *et al*, 2013, 2020). Finally, we performed 10 ML inference replicates, to control for potential instability in the topology, in particular within the EG.5.1.1 lineage.

Visualizations

The plots were created using matplotlibv3.6.3(Hunter, 2007)and the tree was visualized using baltic (https://github.com/evogytis/baltic).